© 2018. Published by The Company of Biologists Ltd | Journal of Experimental Biology (2018) 221, jeb174995. doi:10.1242/jeb.174995

RESEARCH ARTICLE

Vultures respond to challenges of near-ground thermal soaring by varying bank angle

Hannah J. Williams[1,*], Olivier Duriez[2], Mark D. Holton[1,3], Giacomo Dell'Omo[4], Rory P. Wilson[1] and Emily L. C. Shepard[1]

ABSTRACT

Many large birds rely on thermal soaring flight to travel cross-country. As such, they are under selective pressure to minimise the time spent gaining altitude in thermal updrafts. Birds should be able to maximise their climb rates by maintaining a position close to the thermal core through careful selection of bank angle and airspeed; however, there have been few direct measurements of either parameter. Here, we apply a novel methodology to quantify the bank angles selected by soaring birds using on-board magnetometers. We couple these data with airspeed measurements to parameterise the soaring envelope of two species of *Gyps* vulture, from which it is possible to predict 'optimal' bank angles. Our results show that these large birds respond to the challenges of gaining altitude in the initial phase of the climb, where thermal updrafts are weak and narrow, by adopting relatively high, and conserved, bank angles (25–35 deg). The bank angle decreased with increasing altitude, in a manner that was broadly consistent with a strategy of maximising the rate of climb. However, the lift coefficients estimated in our study were lower than those predicted by theoretical models and wind-tunnel studies. Overall, our results highlight how the relevant currency for soaring performance changes within individual climbs: when thermal radius is limiting, birds vary bank angle and maintain a constant airspeed, but speed increases later in the climb in order to respond to decreasing air density.

KEY WORDS: *Gyps* vulture, Aeronautical theory, Circling envelope, Magnetometry, Biologging, Thermal updraft

INTRODUCTION

Many large soaring birds rely on thermal updrafts to cover the large distances required to search for food (Ruxton and Houston, 2004) or complete long migrations (Alerstam et al., 2003; Shamoun-Baranes et al., 2003; Leshem and Yom-Tov, 1996). For the heaviest of these birds, movement across the landscape is completely dependent on their ability to exploit such sources of energy rather than use flapping flight, owing to the way that the costs of powered flight scale with body mass (Hedenström and Alerstam, 1995; Hedenström, 1993). Thermal soaring can be broken down into two different phases: the climb within an updraft, and the glide to the next. In order to maximise the cross-country speed (the overall speed they achieve over ground), birds should minimise the time in both phases, using different strategies to increase their speed in the glide and their climb rate when soaring. Although a wide range of studies has examined the speeds that birds select in inter-thermal glides, and how they vary according to factors such as environmental conditions and experience (Horvitz et al., 2014; Taylor et al., 2016; Harel et al., 2016b; Vansteelant et al., 2017), very few studies have examined how individuals maximise their climb rate within a thermal.

The climb rates that can be achieved within thermal updrafts are determined by (i) the morphology of the bird (Pennycuick, 2008), (ii) the thermal environment that the bird is soaring within and (iii) the bird's behavioural response to this environment (Pennycuick, 2008; Ákos et al., 2010). When it comes to morphology (point i), aeronautical models can be used to predict how fast a bird will sink in still air, which changes with both speed (in a manner described by the glide polar) and bank angle (as described by the circling envelope). In order to maximise its climb rate, a bird should fly at its 'minimum sink' speed. There are also predictions about the bank angles that birds should adopt. Pennycuick modelled the circling envelopes for soaring birds and calculated the optimal bank angle for vultures as approximately 24 deg (Pennycuick, 1971; Flight software, http://www.bristol.ac.uk/biology/media/pennycuick.c/Flight_122_ReadMe.txt). Indeed, such angles have been observed from gliders (e.g. Shannon et al., 2002) and in Himalayan vultures (*Gyps himalayensis*) flying at low altitudes (Sherub et al., 2016). However, the predicted 24 deg is arrived at by assuming that birds are aiming to minimise both their turn radius (and thus remain near the 'core' of the thermal with the strongest uplift) and their sink rate. Although this is reasonable when considering how birds should behave on average, i.e. when considered across thermals, it does not account for the fact that the thermal environment (point ii above) changes with altitude. At low altitudes, thermal updrafts are both weak and narrow, and we predict that birds should select higher bank angles, with their accompanying higher sink rates, allowing them to exploit stronger uplift closer to the thermal core.

Overall, therefore, it is unclear how birds behave given the trade-off between the need to circle tightly and climb rapidly. This is particularly pertinent in marginal conditions, e.g. in the morning, when thermals are relatively weak (Spiegel et al., 2013b; Shannon et al., 2002). The aim of this study was to obtain direct and continuous measurements of bank angle in order to (1) compare these values with theoretical predictions and (2) ascertain whether and how birds vary their bank angle through the thermal climb. Few studies have quantified bank angle directly, although some in-flight angular measurements have previously been recorded incidentally using on-board cameras, for example, to quantify the lateral displacement of the tail in the flight manoeuvres of a steppe eagle, *Aquila nipalensis* (Gillies et al., 2011). Turning radii can also be derived using GPS data (adjusted for wind drift) or measures of airspeed (Treep et al., 2016; Weinzierl et al., 2016; Horvitz et al.,

[1]Department of Biosciences, College of Science, Swansea University, Swansea SA2 8PP, UK. [2]CEFE UMR 5175, CNRS, Université de Montpellier, Université Paul-Valéry Montpellier, EPHE, 1919 route de Mende, 34293 Montpellier Cedex 5, France. [3]Computational Foundry, College of Science, Swansea University, Swansea SA2 8PP, UK. [4]Ornis italica, Piazza Crati 15, 00199 Rome, Italy.

*Author for correspondence (h.williams@swansea.ac.uk)

H.J.W., 0000-0002-6338-529X; O.D., 0000-0003-1868-9750; G.D., 0000-0002-9601-9675

Received 27 November 2017; Accepted 11 October 2018

Journal of Experimental Biology (2018) 221, jeb174995. doi:10.1242/jeb.174995

2014; Sherub et al., 2016). However, deriving bank angle from these measures of turn radius assumes that birds adopt the angles that are required for theoretically ideal circling flight (cf. Pennycuick, 2008). Here, we use a novel method to quantify bank angle directly, based on an on-board magnetometer, and combine this with measurements of airspeed and circling radii to examine individual variation in soaring behaviour through the thermal climb.

MATERIALS AND METHODS

Study system

Data were collected from four individual vultures [Himalayan griffon vulture, *Gyps himalayensis* Hume 1869, n=2; European griffon vulture, *Gyps fulvus* (Hablizl 1783), n=2; all >2 years] at the Rocher des Aigles falconry centre, Rocamadour, France. Here, vultures were released from their perches to fly freely three times a day (at 11:30, 13:00 and 14:00 h local time) in a protocol repeated over 3 days of data collection, totalling nine flights for each vulture (see Table 1 for a summary). This protocol provided an opportunity to quantify the flight performance of birds in semi-captive conditions, at a site with relatively good thermal soaring conditions (see Duriez et al., 2014 for details). Wing loading (kg m^{-2}) was derived from measurements of body mass (kg) and total wing area (m^2) (the latter was calculated from photographs of fully extended wings on a scaled background), as turning radius increases with wing loading (Ákos et al., 2010; Pennycuick, 1971).

Device deployment

Vultures were fitted with Daily Diary loggers (DD, recording at 40 Hz) and GPS units (recording position at 4 Hz), which were attached with a Teflon leg-loop harness (Fig. 1) at the beginning of data collection (approximately 90 g, ∼1.2% body weight). The harness remained in place for the following 5 days. The harness held an aluminium plate, which was positioned on the lower back, and aligned with the spine. Devices were attached to the plate using Velcro and were deployed prior to the first flight of the day and removed at the end of each day. The permit for equipping vultures with loggers was provided as part of the licence of O. Duriez from the Research Centre for Bird Population Studies (CRBPO) of the French National Museum of Natural History (MNHN, Paris). Birds were handled by their usual trainer, under the permit of the Rocher des Aigles.

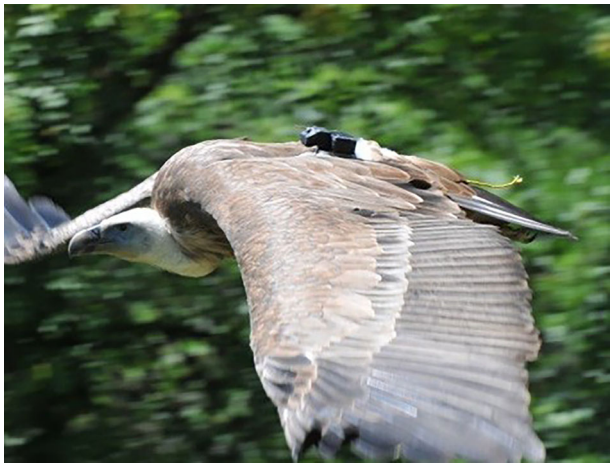

Fig. 1. Griffon vulture in flight, wearing a leg loop harness and tags (Daily Diary; GPS).

DD units (Wilson et al., 2008) were programmed to record the following parameters at 40 Hz: acceleration ($\boldsymbol{g}$) in three axes, geomagnetic field strength (Gauss), also in three axes, barometric pressure (Pa) and temperature. The DD also incorporated a differential pressure sensor, with dynamic pressure recorded through a forward-facing Pitot tube (brass with a bore diameter of 2.5 mm) that extended outside the housing to measure uninterrupted airflow (see Williams et al., 2015 for details).

Derivation of angle using the magnetometer

Acceleration and barometric pressure data were used to identify the times of take-off and landing (barometric pressure also being used to calculate altitude, see below). It is important to note that although accelerometers can be used to measure postural rotation in many terrestrial systems, they cannot be used to measure bank angle in flight, and in particular soaring flight, owing to the centripetal acceleration (see Williams et al., 2015). Thermal soaring flight was defined by a sustained increase in altitude (measured as a decrease in air), the presence of a consistent sine wave in the x- and z-axes of the TriMag data, indicating circling behaviour (Williams et al., 2015), and the distinct lack of flapping (as would be indicated by peaks in

Table 1. Summary flight statistics for the four tagged vultures

Individual	A	B	C	D
Species	*Gyps himalayensis*	*Gyps himalayensis*	*Gyps fulvus*	*Gyps fulvus*
Sex	Female	Female	Male	Male
Age	Subadult	Adult	Subadult	Subadult
Wing loading	6.63	7.18	7.06	7.28
Body mass (kg)	8.45	8.10	7.20	7.15
Wing area (m^2)	1.27	1.13	1.02	0.98
Aspect ratio	5.98	6.95	6.73	6.88
No. flights	3, 3, 3	3, 3, 3	3, 3, 2	3, 3, 2
Total flight (min)	22.01±10.35	26.77±9.17	17.45±9.83	17.59±7.49
Circling (%)	54±10	49±9	54±6	51±7
Max. altitude (m)	847.72±380.88	898.20±334.01	702.93±382.14	707.24±350.35
No. complete turns	146, 73, 115 Total=334	122, 122, 115 Total=359	131, 92, 32 Total=255	85, 84, 38 Total=207
Climb rate (m s^{-1})	0.99±0.90	1.25±1.21	0.91±0.99	0.83±0.82
Bank angle (deg)	26.54±7.58	29.38±7.29	31.74±8.29	35.78±10.24
Average airspeed (m s^{-1})	13.21±0.03	13.51±0.03	12.89±0.05	14.15±0.09
Lift coefficient (C_L)	0.79±0.20	0.82±0.20	0.94±0.23	0.73±0.17

The number of flights and total flight time include all time spent in the air, all other flight parameters are specific to the thermal soaring periods. Values are given as means±s.d. for total flight, circling, maximum altitude and average airspeed, and as medians±IQR for climb rate, bank angle and C_L. For the number of flights and complete turns, values are given for the three release times through the day: 11:30, 13:00 and 14:30 h, respectively.

Journal of Experimental Biology (2018) 221, jeb174995. doi:10.1242/jeb.174995

dynamic acceleration). Complete turns were selected from all thermal soaring periods, where individual turns were defined as the period between two consecutive peaks in the *x*-axis.

Estimates of bank angle were derived from the TriMag data as follows, assuming that the bank of the body reflected the bank angle adopted by the wings (this was supported by preliminary work with a camera showing the bank of the wing was consistent relative to the body; Fig. S1). Data from each of the three magnetometer channels can be plotted in 3D space and normalised to a spherical surface defined as the m-sphere (Williams et al., 2017). Plotting a single 360 deg rotation for a given bank angle produces an individual ring on the m-sphere (Fig. 2). The centroid of this ring, that is, the *x*, *y* and *z* coordinates of the central point of the ring on the surface of the sphere, gives the average bank angle over the course of the complete turn. This was determined by calculating the difference between the dot product of the *x*, *y* and *z* coordinates of a given centroid, and the point of 0 deg bank [i.e. (0, −1, 0)] using:

$$\theta = \left(\frac{180}{\pi}\right) \times \operatorname{acos}\left[\frac{(0x - 1y + 0z)}{(x^2 + y^2 + z^2)\sqrt{(0^2 + -1^2 + 0^2)}}\right], \quad (1)$$

where *x*, *y* and *z* are the coordinates of the TriMag centroid for a complete turn.

Plotting the distribution of bank angles estimated using the TriMag approach highlighted skews in the data, suggesting the tags were not perfectly aligned with the sagittal plane of the bird. The exact orientation of the device was not known, and is likely to have differed slightly between birds and days of attachment, causing an overestimation of bank in one direction of turn and an underestimation in the other. Consequently, the data were re-aligned so that the crossing point between turns of opposing direction corresponded to a 0 deg angle of bank. This therefore assumed that turns of opposing direction had similar ranges in bank angle, analogous to the transformations of Gillies et al. (2011). Centroid angles were recalculated for all flights following realignment. All subsequent analyses of bank angle were made using the re-aligned TriMag data. The processing and analysis of TriMag data were performed with the custom-built software DDMT (Wildbytes Technology Ltd, Swansea University).

Derivation of soaring parameters

The radius of each complete turn was calculated from the average airspeed of the turn and turn duration. Previous studies have measured turn radius using GPS corrected for wind drift (e.g. Weinzierl et al., 2016; Treep et al., 2016). By using the airspeed, we can derive radius from the reference frame of the bird, removing the effect of drift on its path. To derive the airspeed, we converted the differential pressure output from volts to true airspeed (V_t) in metres per second. This relationship was derived by selecting 5-s straight-line sections of gliding flight and calculating the airspeed (V_a) in these periods according to the triangle of velocities, using the equation:

$$V_a^2 = V_g^2 + V_w^2 + 2V_g V_w \cos\gamma, \quad (2)$$

where V_g and V_w are the groundspeed (from the 4 Hz GPS) and wind speed vectors, respectively, and γ is the angle between them. The wind vector was specific to each glide, being estimated from drift in the previous thermal just minutes beforehand (via the GPS track by taking the straight-line distance between the corresponding points of complete turns, and dividing by time; see Treep et al., 2016). We used separate linear regressions to calibrate V_t for each bird. These predicted V_t from V_a, as well as V_a in interaction with day (where significant), to account for the fact that the position of the logger could vary between days. This approach allowed us to determine the airspeed, V_t, at 40 Hz through the entire flight.

The climb rate (m s^{-1}) per turn was taken as the difference in altitude from the start to the end point of the turn, divided by turn duration, where altitude was derived from the barometric pressure (smoothed over 10 s), assuming standard atmospheric conditions. The daily mean sea level pressure was taken from the nearest weather station at Lunegarde, 20 km from the study site.

Each individual's circling envelope was parameterised using measured angles of bank (θ) and turn radii (*r*), and the lift coefficient (C_L), estimated by rearranging:

$$r = \frac{2m}{(C_L \times \rho \times S \times \sin\theta)}, \quad (3)$$

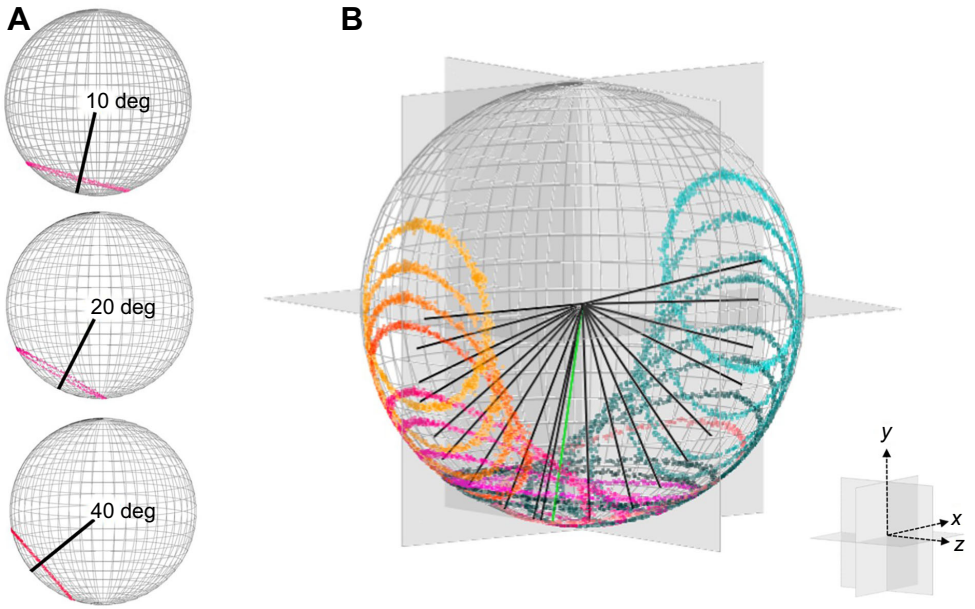

Fig. 2. Tri-axial magnetometry data normalised to a spherical surface (the m-sphere). (A) Complete rotations of the magnetometer appear as circles on the sphere, with the line from the centre of the m-sphere to the centroid of each circle indicating the mean angle of bank in a given turn. (B) A calibration device was used to simulate a bird circling with fixed bank angles varying from −90 (yellow) to 90 deg (light blue) at 10 deg intervals, indicative of left and right banked turns, respectively. The m-print that corresponds to zero bank is at the bottom of the m-sphere. Units were calibrated using this device in the field, with the camera and GPS units also attached to the platform [as these could potentially influence the magnetometer data (see Bidder et al., 2015)].

Journal of Experimental Biology (2018) 221, jeb174995. doi:10.1242/jeb.174995

where m is the mass of the bird (kg), ρ is the air density in 100 m bins under normal conditions and S is the wing area. Using the median C_L for the bird, we then compared the envelope derived from empirical data with that predicted by Pennycuick's model in the Flight software. To validate our median lift coefficient, we also calculated the C_L in terms of the induced drag (D_i) using the following equations:

$$D_i = mg(\sin\varphi) - \frac{1}{2}\rho V_t^2 D_0 S, \quad (4)$$

$$C_L = \sqrt{\frac{2D_i \pi AR}{SV_t^2 \rho k}}, \quad (5)$$

where mg is the weight of the bird, ϕ is the assumed angle of attack at 15 deg, ρ is mean air density, V_t is the mean true airspeed, D_0 is the profile drag at Pennycuick's constant of 0.114 (Pennycuick, 1971), k is the induced power factor at 1.2 [a commonly used conservative value (see Klein Heerenbrink et al., 2015) that accounts for the wings not being perfectly elliptical] and AR is the aspect ratio.

Data analyses

Kruskal–Wallis tests were used to assess individual variation in bank angle and associated climb rate across flights. We examined variation in airspeed with altitude using a linear mixed-effects model (LMM) with the random effects of day nested within individual ID. Individual variation in bank angle and climb rate was examined in relation to altitude. Initial inspection of the data suggested that, for each vulture, climb rate levelled off with altitude, with a breakpoint in the height at which this occurred. We therefore performed a segmented analysis to identify breakpoints in the individual-specific linear relationships between the climb rate and altitude (R software, 'segmented' package; Muggeo, 2003). Data were restricted to ≤1000 m for the segmented analysis as birds rarely exceeded this height. The relationship between climb rate and altitude was then compared before and after the identified breakpoint. We did not compare the results in terms of species or age (we did not believe individuals would dramatically differ in soaring performance owing to age alone given that all birds were >2 years old; see Harel et al., 2016a), but focused on within-individual trends in climb rate and bank angle, thus allowing us to examine changes in soaring behaviour through the climb. However, we did consider the effects of wing loading on soaring behaviour, as wing loading is the main morphological factor that is known to have significant impact on the limits of the circling envelope.

Finally, we examined climb rate in relation to distance from the thermal core using the empirically parameterised circling envelope and data collected from a single focal individual (this being the individual where the regression analyses of V_t by V_a accounted for most variance). Assuming a normal distribution of vertical velocities, we estimated the maximum climb rate that could be achieved for a given thermal region (i.e. height and radius), partitioning the thermal into low (200–400 m), mid (400–600 m) and high (>600 m) regions (high being altitudes above the individual's breakpoint; see Results). All analyses were performed in R 3.2.3.

RESULTS

Overall, 34 flights were recorded across the 3 days of data collection (*G. himalayensis*, 9 flights each; *G. fulvus*, 8 flights each; Table 1). Flights ranged from 5.28 to 45.27 min (mean=20.96±s.d. 9.63 min). Flights performed in the first release of the day at

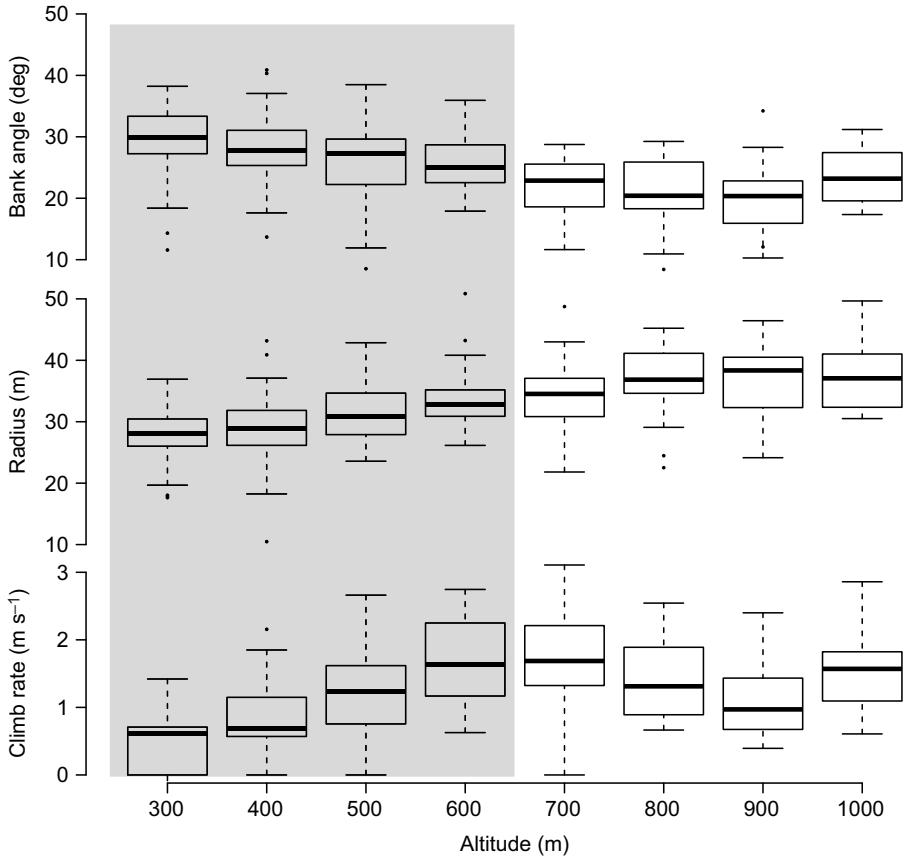

Fig. 3. Trends in bank angle, turning radius and achieved climb rate, binned according to altitude above sea level (100 m bin width) for the *Gyps himalayensis* subadult. The shaded region highlights the low-altitude region below the modelled breakpoint for this bird (515.91±22.86 m), where an increase in climb rate occurred as birds decreased their bank angle (n=334). This trend does not hold beyond the breakpoint in any bird (Table S2).

Journal of Experimental Biology (2018) 221, jeb174995. doi:10.1242/jeb.174995

Table 2. Relationship between climb rate and altitude before and after the identified breakpoint in the climb

Bird ID	Breakpoint (m)	
A	509.85±26.18	**Low: r_S=0.621, *N*=214, *P*<0.001**
		High: r_S=−0.024, *N*=120, *P*=0.792
B	463.13±32.83	**Low: r_S=0.582, *N*=206, *P*<0.001**
		High: r_S=0.261, *N*=153, *P*=0.001
C	680.17±69.56	**Low: r_S=0.451, *N*=212, *P*<0.001**
		High: r_S=−0.069, *N*=43, *P*=0.657
D	607.00±72.17	**Low: r_S=0.398, *N*=180, *P*<0.001**
		High: r_S=−0.049, *N*=27, *P*=0.806

Spearman's rank correlation test for low and high thermal regions (significant relationships in bold) using data prior to and following the breakpoints identified from their corresponding models (Table S2).

11:30 h tended to be longer and reach greater altitudes than those of subsequent releases (flight 1: 11:30 h, 27.04±10.06 min, 609.84±323.10 m; flight 2: 13:00 h, 19.21±6.01 min, 424.62±150.38 m; flight 3: 14:30 h, 14.44±8.82 min, 445.86±193.48 m). A total of 1155 complete thermal turns were isolated for bank angle analyses (per individual: 289±70; Table 1). Angles differed significantly between all four individuals (Kruskal–Wallis χ^2=262.650, d.f.=3, *P*<0.001), with median bank angles ranging between 25 and 35 deg (Table 1). Regression analyses found a significant relationship between V_a (measured from the triangle of velocities) and the raw differential pressure values for each bird (Pitot), from which conversion equations were derived (focal bird A, V_a=0.0047×Pitot–28.33, in a regression with an adjusted R^2 of 0.71; the remaining birds are presented in Fig. S2, Table S1). V_t did not change through the climb when examined in relation to altitude (LMM χ^2=1.436, d.f.=5.1, *P*=0.231), allowing us to assume a direct relationship between time to complete the turn and its radius (individual airspeeds reported in Table 1).

Overall, birds decreased their bank angle (Spearman's rank correlation, r_S=−0.467, *N*=1155, *P*<0.001) and increased their turning radius (Spearman's rank correlation, r_S=0.676, *N*=1155, *P*<0.001) with altitude (Fig. 3), in a manner consistent with a movement along the circling envelope. There was also a general increase in climb rate with altitude, with one significant break in this relationship for each of the four individuals (the average breakpoint was 560±41 m across all birds; Table S2). The relationship between climb rate and altitude was highly conserved before the breakpoint (e.g. for the bird shown in Fig. 3: r_s=0.621, *N*=214, *P*<0.001), but variable, and with a lack of correlation, after the breakpoint (r_s=−0.024, *N*=116, *P*=0.792; Table 2).

The birds occupied a space within their theoretical circling envelope as predicted by the theoretical maximal lift coefficient (Fig. 4A). In fact, the overall agreement was very good, in terms of the empirical data being apparently bounded by the theoretical envelope. However, there was some variation in sink rate for a given combination of circling radius and bank angle, with birds operating below their theoretical optima (i.e. at a lower lift coefficient). This decrease in performance did not seem to be related to the wind vector (Fig. 4B) or the time or day of the flight. Instead, it is likely to reflect the relatively high airspeeds adopted by these birds, which were typically 13–14 m s^{-1}, compared with the predicted minimum sink speeds of up to 9 m s^{-1}.

The lift coefficients that birds generally operated at were lower than the theoretical C_L at minimum sink (ranging from 1.37 to 1.47), irrespective of the method used. When the empirical values of bank angle and turn radius were used, average lift coefficients were estimated to be 0.73 and 0.94 for the two *G. fulvus* individuals and 0.79 and 0.82 for the two *G. himalayensis* individuals. The C_L calculated from the biometric data, average airspeed and Pennycuick's drag constants was equally low, e.g. 0.81, for the focal bird (Fig. 4A). The consequences of the lower C_L mean that this individual had an average limiting turn radius of 13.68 m, compared with a radius of 7.9 m with a theoretical C_L of 1.37.

DISCUSSION

In this study, we use novel techniques to measure bank angle and turn radius using animal-attached loggers. Our method of obtaining bank angle capitalises on the inherently three-dimensional nature of magnetometry data, which can be normalised to the surface of a

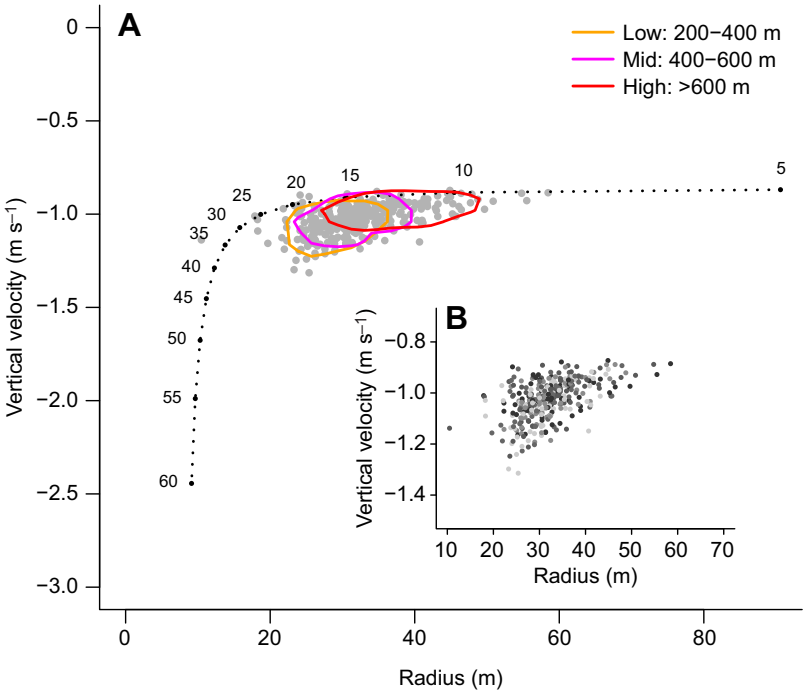

Fig. 4. Vertical veolcity (m s^{-1}) achieved in thermal soaring in relation to the adopted turning radii (m) and average bank angles (deg). (A) The circling envelope for vulture A, the *Gyps himalayensis* subadult, parameterised using empirical data (grey dots) of bank angle and turning radius (*n*=334). With increasing radius and decreasing bank angle the bird's own sink rate decreases (labelled as negative vertical velocity). The bird shifts along this envelope from high bank angles and tight turning radii to a region of low angles and greater turning radii, decreasing its sink rate with altitude (0.9 polygons). Although the empirical data sit within the envelope predicted by the Pennycuick model (dotted line) (Pennycuick, 2008), which assumes a lift coefficient (C_L) of 1.37, actual turning radii were greater than predicted for a given angle of bank. This produces a higher estimate of the average limiting turn radius (13.68 m), given a median C_L of 0.79. (B) The relationship between sink rate, bank angle and turning radius does not appear to be related to wind speed (gradient of light to dark grey with increasing wind speed).

Journal of Experimental Biology (2018) 221, jeb174995. doi:10.1242/jeb.174995

sphere (when measurements are made in all three axes). We show that, for a complete turn in thermal soaring, the rotation in heading defines a circular ring on the sphere, and the position of this ring is determined by the animal's posture (Williams et al., 2017). As vultures show relatively little variation in pitch during thermal soaring, changes in the position of the circle result from rotation in the roll axis. The use of three-dimensional magnetometry data therefore allows us to quantify bank angle for prolonged periods of time, with the advantages of minimal calibration and post-processing in comparison with camera methods (used here to validate the magnetometry method in preliminary analyses). Gyroscopes in on-board devices can also be used to measure angular movement (e.g. Martín López et al., 2016; Noda et al., 2014; Wilson et al., 2013); in practice, however, gyroscopes are not well suited to continuous data collection on free-living animals, owing to their relatively high current draw (a problem that also limits the use of cameras).

Early work by Pennycuick (1971) proposed that *Gyps* vultures should adopt bank angles of between 20 and 40 deg. Our measurements generally align with these theoretical predictions, in terms of the median bank angles adopted. Nonetheless, birds were somewhat conservative in the maximum angles they used. That is, although they tended to select angles up to 35 deg, they could, according to the theoretical circling envelope, increase their bank angles by a further ∼5 deg before incurring substantial penalties in sink rate. Adopting tight turning radii may be associated with the risk that small control inputs could cause a bird to 'overbank' and move into an area of performance space with high sink rates, thus compromising climb performance. This is the first work that does not assume that these birds are operating at the limits of their performance, but rather examines the distribution of data within the circling envelope to investigate within-individual variation in performance, an approach that could be developed further to provide insight into individual strategies or interspecific variation. It is interesting to note that the adult female maintained average climb rates at least 25% greater than other birds in this study, as well as the lowest variance in bank angle overall. This increased performance and consistency may be an indicator of soaring skill acquired through greater experience (see Harel et al., 2016a).

Thermal updrafts tend to be narrower and weaker when close to the ground, expanding as they rise. Optimising soaring performance at low altitudes is therefore critical in order to gain sufficient altitude to glide to the next thermal (Pennycuick, 2008). Indeed, it has been recognised since the 1960s (e.g. Kruuk, 1967) that the activity rhythms of soaring birds are determined by the mass of the bird in relation to the strength of thermal updrafts, with larger birds only able to gain altitude later in the day when thermals are stronger (see Spiegel et al., 2013b). Birds in the present study displayed marked changes in bank angle with altitude, decreasing from around 30 to 22 deg in the first few hundred metres of the climb, and increasing their turn radii in a manner generally consistent with the circling envelope (i.e. the optimal solution for climbing performance). The relatively tight relationship between bank angle, climb rate and altitude in the first few hundred metres demonstrates the importance of changes in bank angle in enabling soaring birds to gain altitude when close to the ground.

Our finding that birds modulate radius by changing bank angle is in contrast to that of a recent study on Himalayan griffon vultures soaring in excess of 6000 m (Sherub et al., 2016). Although the Himalayan griffons also increased their radius with altitude, they achieved this by increasing their airspeed (keeping bank angle constant). This increase in radius and airspeed is necessary to compensate for the decreasing air density over a dramatic altitudinal range. Interestingly, therefore, soaring birds appear to vary their circling radius by two different mechanisms according to the flight

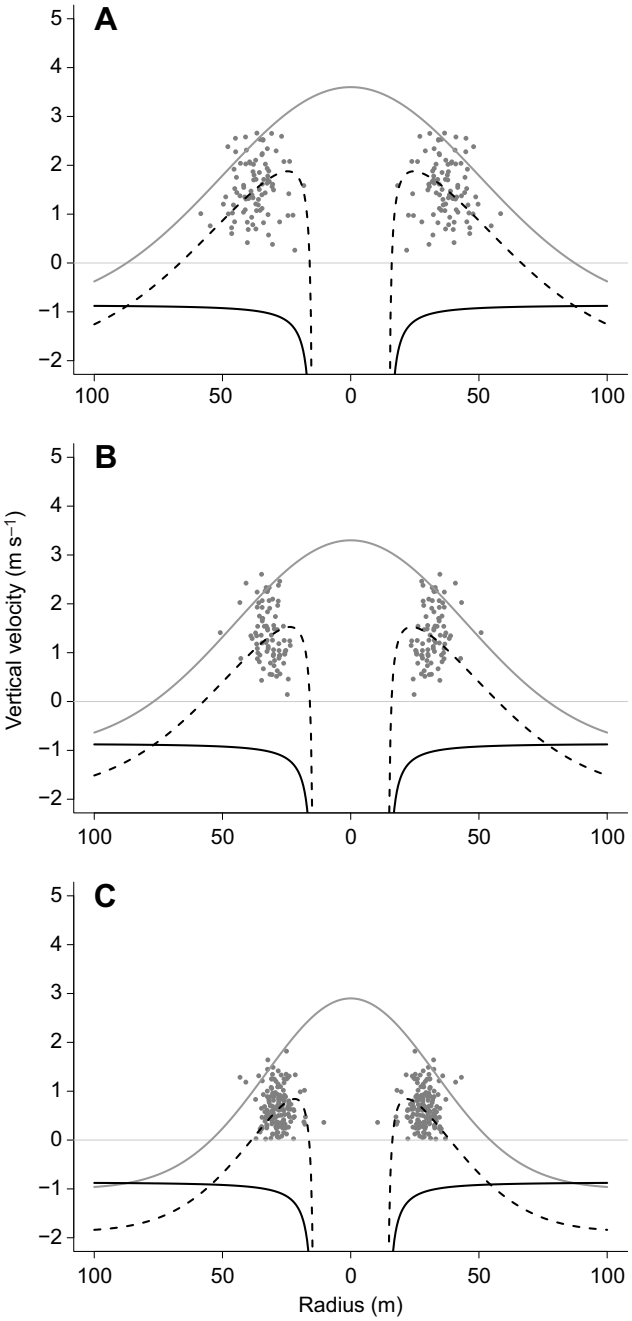

Fig. 5. The velocity profile of a thermal updraft at three altitudes, as modelled from the climb rates, radii and circling envelope for the *Gyps himalayensis* subadult. When soaring, the thermal's upward vertical velocity (solid dark grey line) exceeds that of the bird's downward velocity, so that the bird experiences a positive climb rate. Hence the thermal velocity is taken as the sum of the bird's mean climb rates (raw data shown by grey points) and estimated sink rates for three regions: (A) high: >600 m, (B) mid: 400–600 m and (C) low: 200–400 m. This is then interpolated across the thermal diameter assuming a normal distribution of uplift. The bird's circling envelope (solid black line) and the rate at which air is rising within the thermal define the area within which the bird is able to position itself and gain height. This area is where the climb rate (dashed line) is >0 m s^{-1} (horizontal line). Achievable climb rates drop dramatically close to the core of the updraft owing to the sink rates associated with high bank angles.

altitude. This dual strategy demonstrates the complexity involved in maximising height gain and leads to the question of when and how birds should switch strategy through the climb. With little height above the ground, the priority has to be maximising the climb rate. It seems most likely that birds increase their airspeed at or above the point at which thermal radius is no longer the primary constraint.

In our system, there was a breakpoint in the relationship between climb rate and altitude at approximately 560 m. As turn radius increases, birds experience diminishing returns in sink rate. Vertical velocity above the breakpoint is therefore less likely to be linked to variation in bank angle, but rather to the thermal conditions, which may also vary between days. Because the birds used here do not roam far during their flights, it could also be that they have no need to gain height beyond that required to return to their home destination. Nonetheless, we see no clear advantage in maintaining, rather than increasing, altitude, should the thermal structure allow (but see Shannon et al., 2002).

Although the variation in bank angle with altitude that we observed was consistent with a tendency to maximise the climb rate, the average lift coefficient was 52% of the theoretical maximum (it was also less than the C_L observed for a jackdaw soaring at its minimum sink speed in a wind tunnel; e.g. Rosén and Hedenström, 2001). Our measurements of C_L could have been influenced by factors that fall into three main categories: (i) methodological, (ii) environmental and (iii) behavioural (Fig. 5). In terms of the methodology, although a low lift coefficient may be the result of an overestimated bank angle or turning radius (the latter could result from an overestimated airspeed), the fact that our data did not cross the theoretical circling envelope supports the idea that they are accurate, as do our data checks, which resulted in an equally low lift coefficient. When it comes to behaviour, these birds were often recorded flying at airspeeds that were higher than the theoretically predicted minimum sink speeds (which is also likely linked to their conservative bank angles; see above). Actual flight speeds were more similar to those recorded in inter-thermal glides in previous work (recorded at an average of 16.5 m s^{-1} by Harel et al., 2016b), which could therefore explain the low C_L values. In terms of environmental parameters, we found no clear relationship between wind or time of day and position within the envelope. However, although there was no evidence of the C_L varying with wind strength, it may be that wind affects soaring performance in a complex way (e.g. Harel et al., 2016a).

Overall, we show that the constraints on soaring flight vary with altitude, and that this results in birds modulating their circling radius in relation to two different factors. At low altitudes, obligate soaring birds select relatively steep bank angles to maintain their position in a narrow region of strong uplift (Fig. 5). However, although the circling envelope appeared to be predicted well by theoretical models, we demonstrate that it cannot be assumed that soaring birds are operating at their theoretical optima, and that performance may be influenced by additional factors. Longer-term data from free-ranging individuals could provide insight into how the bank angles selected during the critical, near-ground phase of soaring may vary with experience (cf. Harel et al., 2016a) and state variables such as hunger (Nathan et al., 2012; Spiegel et al., 2013a), which may provide an incentive for birds to operate in more marginal conditions or select higher bank angles.

Acknowledgements
We would like to thank D. Maylin and R. Arnaud, directors at the Rocher des Aigles (Rocamadour, France), and all of their staff for their patience and interest in the project. We are extremely grateful for their enthusiasm, keen interest in the project and willingness to work this data collection protocol into their daily routine. We also thank S. Potier and J. Fluhr for their help with tag deployments. DD housings were designed by P. Hopkins. H.J.W. would also like to thank C. Rees-Roderick for fruitful discussions.

Competing interests
The authors declare no competing or financial interests.

Author contributions
Conceptualization: H.J.W., E.L.S.; Methodology: H.J.W., M.D.H., R.P.W., E.L.S.; Software: M.D.H.; Validation: M.D.H.; Formal analysis: H.J.W.; Investigation: H.J.W., O.D.; Resources: O.D., G.D., R.P.W., E.L.S.; Data curation: H.J.W.; Writing - original draft: H.J.W.; Writing - review & editing: H.J.W., O.D., M.D.H., G.D., R.P.W., E.L.S.; Visualization: H.J.W.; Supervision: E.L.S.; Project administration: H.J.W., O.D., E.L.S.

Funding
H.J.W. was supported by a Swansea University studentship during data collection through to completion of the manuscript.

Data availability
All data collected from the on-board devices can be accessed in the Movebank study '*Gyps* vultures with Pitot airspeed at Rocamadour' and are available from the Movebank data repository: doi:10.5441/001/1.4f03k6s5.

Supplementary information
Supplementary information available online at
http://jeb.biologists.org/lookup/doi/10.1242/jeb.174995.supplemental

References
Ákos, Z., Nagy, M., Leven, S. and Vicsek, T. (2010). Thermal soaring flight of birds and unmanned aerial vehicles. *Bioinspir. Biomim.* **5**, 045003.
Alerstam, T., Hedenström, A. and Åkesson, S. (2003). Long-distance migration: evolution and determinants. *Oikos* **103**, 247-260.
Bidder, O. R., Walker, J. S., Jones, M. W., Holton, M. D., Urge, P., Scantlebury, D. M., Marks, N. J., Magowan, E. A., Maguire, I. E. and Wilson, R. P. (2015). Step-by-step: reconstruction of terrestrial animal movement paths by dead-reckoning. *Mov. Ecol.* **3**, 23.
Duriez, O., Kato, A., Tromp, C., Dell'omo, G., Vyssotski, A. L., Sarrazin, F. and Ropert-Coudert, Y. (2014). How cheap is soaring flight in raptors? A preliminary investigation in freely-flying vultures. *PLoS ONE* **9**, e84887.
Gillies, J. A., Thomas, A. L. R. and Taylor, G. K. (2011). Soaring and manoeuvring flight of a steppe eagle *Aquila nipalensis*. *J. Avian Biol.* **42**, 377-386.
Harel, R., Horvitz, N. and Nathan, R. (2016a). Adult vultures outperform juveniles in challenging thermal soaring conditions. *Sci. Rep.* **6**, 27865.
Harel, R., Duriez, O., Spiegel, O., Fluhr, J., Horvitz, N., Getz, W. M., Bouten, W., Sarrazin, F., Hatzofe, O. and Nathan, R. (2016b). Decision-making by a soaring bird: time, energy and risk considerations at different spatio-temporal scales. *Philos. Trans. R. Soc. B* **371**, 20150397.
Hedenström, A. (1993). Migration by soaring or flapping flight in birds: the relative importance of energy cost and speed. *Philos. Trans. R. Soc. B* **342**, 353-361.
Hedenström, A. and Alerstam, T. (1995). Optimal flight speed of birds. *Philos. Trans. R. Soc. B* **348**, 471-487.
Horvitz, N., Sapir, N., Liechti, F., Avissar, R., Mahrer, I. and Nathan, R. (2014). The gliding speed of migrating birds: slow and safe or fast and risky? *Ecol. Lett.* **17**, 670-679.
Klein Heerenbrink, M., Johansson, L. C. and Hedenström, A. (2015). Power of the wingbeat: modelling the effects of flapping wings in vertebrate flight. *Proc. R. Soc. A* **471**, 20140952.
Kruuk, H. (1967). Competition for food between vultures in east Africa. *Ardea* **55**, 171-193.
Leshem, Y. and Yom-Tov, Y. (1996). The use of thermals by soaring migrants. *Ibis* **138**, 667-674.
Martín López, L. M., Aguilar de Soto, N., Miller, P. and Johnson, M. (2016). Tracking the kinematics of caudal-oscillatory swimming: a comparison of two on-animal sensing methods. *J. Exp. Biol.* **219**, 2103-2109.
Muggeo, V. M. R. (2003). Estimating regression models with unknown break-points. *Stat. Med.* **22**, 3055-3071.
Nathan, R., Spiegel, O., Fortmann-Roe, S., Harel, R., Wikelski, M. and Getz, W. M. (2012). Using tri-axial acceleration data to identify behavioral modes of free-ranging animals: general concepts and tools illustrated for griffon vultures. *J. Exp. Biol.* **215**, 986-996.
Noda, T., Kawabata, Y., Arai, N., Mitamura, H. and Watanabe, S. (2014). Animal-mounted gyroscope/accelerometer/magnetometer: in situ measurement of the movement performance of fast-start behaviour in fish. *J. Exp. Mar. Biol. Ecol.* **451**, 55-68.
Pennycuick, C. J. (1971). Gliding flight of the white-backed vulture *Gyps africanus*. *J. Exp. Biol.* **55**, 13-38.

Pennycuick, C. J. (2008). *Modelling the Flying Bird*. Vol. 5, 1st edn. Boston: Elsevier.
Rosén, M. and Hedenström, A. (2001). Gliding flight in a jackdaw: a wind tunnel study. *J. Exp. Biol.* **204**, 1153-1166.
Ruxton, G. D. and Houston, D. C. (2004). Obligate vertebrate scavengers must be large soaring fliers. *J. Theor. Biol.* **228**, 431-436.
Shamoun-Baranes, J., Leshem, Y., Yom-Tov, Y. and Liechti, O. (2003). Differential use of thermal convection by soaring birds over central Israel. *The Condor* **105**, 208-218.
Shannon, H. D., Young, G. S., Yates, M. A., Fuller, M. R. and Seegar, W. S. (2002). American white pelican soaring flight times and altitudes relative to changes in thermal depth and intensity. *Condor* **104**, 679-683.
Sherub, S., Bohrer, G., Wikelski, M. and Weinzierl, R. (2016). Behavioural adaptations to flight into thin air. *Biol. Lett.* **12**, 20160432.
Spiegel, O., Harel, R., Getz, W. M. and Nathan, R. (2013a). Mixed strategies of griffon vultures' (*Gyps fulvus*) response to food deprivation lead to a hump-shaped movement pattern. *Mov. Ecol.* **1**, 5.
Spiegel, O., Getz, W. M. and Nathan, R. (2013b). Factors influencing foraging search efficiency: why do scarce lappet-faced vultures outperform ubiquitous white-backed vultures? *Am. Nat.* **181**, E102-E115.
Taylor, G. K., Reynolds, K. V. and Thomas, A. L. R. (2016). Soaring energetics and glide performance in a moving atmosphere. *Philos. Trans. R. Soc. Lond. B Biol. Sci.* **371**, 20150398.
Treep, J., Bohrer, G., Shamoun-Baranes, J., Duriez, O., Prata De Moraes Frasson, R. and Bouten, W. (2016). Using high-resolution GPS tracking data of bird flight for meteorological observations. *Bull. Am. Meteorol. Soc.* **97**, 951-961.
Vansteelant, W. M. G., Shamoun-Baranes, J., McLaren, J., van Diermen, J. and Bouten, W. (2017). Soaring across continents: decision-making of a soaring migrant under changing atmospheric conditions along an entire flyway. *J. Avian Biol.* **48**, 887-896.
Weinzierl, R., Bohrer, G., Kranstauber, B., Fiedler, W., Wikelski, M. and Flack, A. (2016). Wind estimation based on thermal soaring of birds. *Ecol. Evol.* **6**, 8706-8718.
Williams, H. J., Shepard, E. L. C., Duriez, O. and Lambertucci, S. A. (2015). Can accelerometry be used to distinguish between flight types in soaring birds? *Anim. Biotelemetry* **3**, 45.
Williams, H. J., Holton, M. D., Shepard, E. L. C., Largey, N., Norman, B., Ryan, P. G., Duriez, O., Scantlebury, M., Quintana, F., Magowan, E. A. et al. (2017). Identification of animal movement patterns using tri-axial magnetometry. *Mov. Ecol.* **5**, 6.
Wilson, R. P., Shepard, E. L. C. Liebsch, N. (2008). Prying into the intimate details of animal lives: use of a daily diary on animals. *Endanger. Species Res.* **4**, 123-137.
Wilson, A. M., Lowe, J. C., Roskilly, K., Hudson, P. E., Golabek, K. A. and Mcnutt, J. W. (2013). Locomotion dynamics of hunting in wild cheetahs. *Nature* **498**, 185-189.

Fig. S1. composite of wing to body position during thermal soaring. Screenshots taken from a camera placed on top of our tag device attached to the lower back of the bird, with the camera facing the tip of the right wing. Video was recorded on multiple days from two different birds and through different thermal climbs, and the shots taken at random. The image clearly shows consistency in the body-to-wing position within and between climbs, and interestingly this was also evident between climbs of differing turn direction. Though they may be capable of changing wing orientation at the shoulder joint, if they did so predominantly in soaring we would expect clockwise turns that show the ground to show very little wing in the image, and anti-clockwise turns where the wing is pointing towards the sky, to fill the image with the wing.

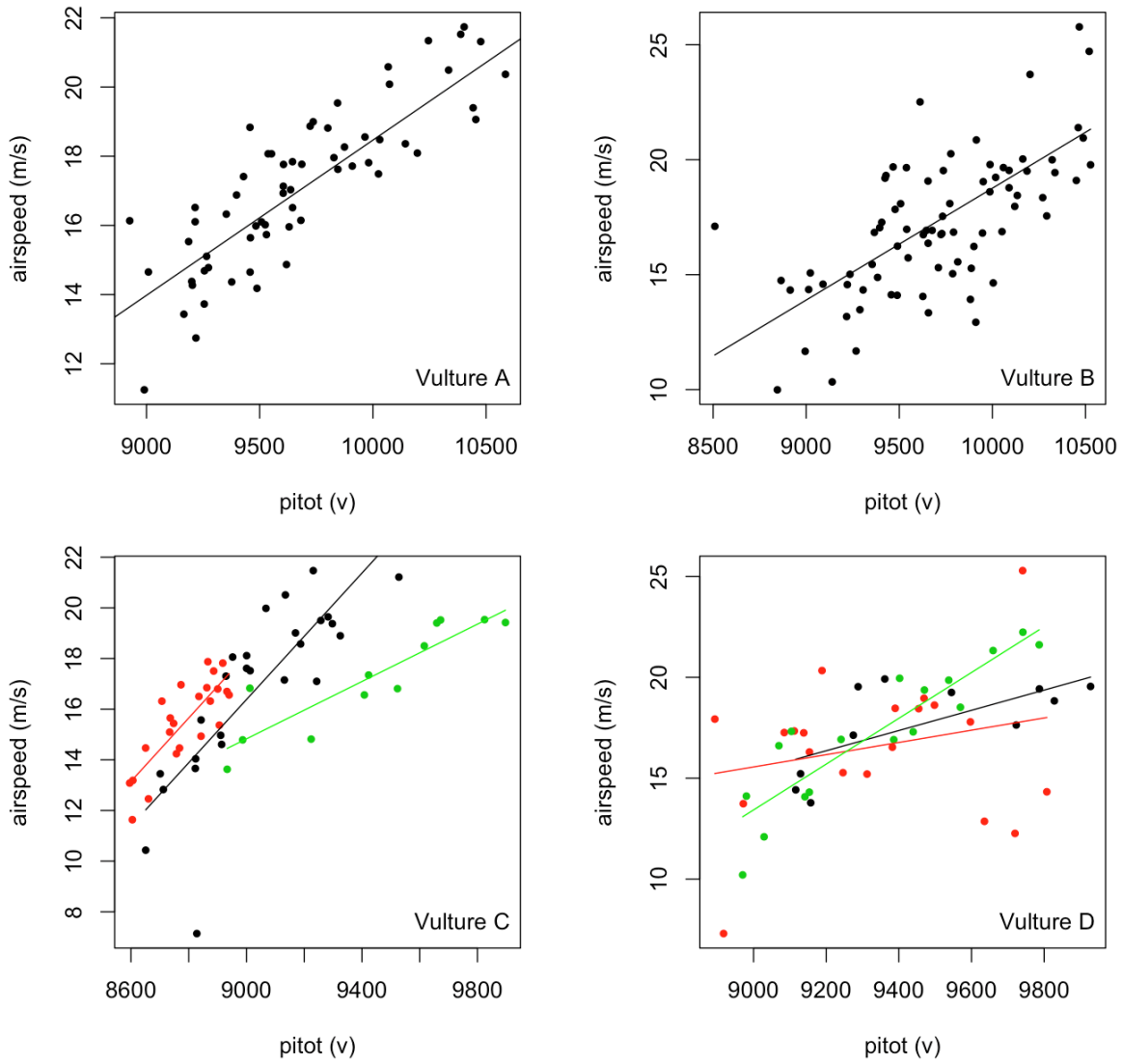

Fig. S2. Regression of the Pitot tube airflow against airspeed derived from the wind and ground speed vectors in gliding. Vulture A (no interaction with day, Adj R^2 =0.71), Vulture B (no interaction, but independent effect of day, Adj R^2 = 0.56), Vulture C (interactive effect of day, Adj R^2 = 0.67), Vulture D (interactive effect of day, Adj R^2 = 0.33).

Table S1. Individual-specific linear regressions predicting airspeed values (V_a) from the corresponding Pitot tube data (volts).

Vulture A		$V_a = 0.004700\mathrm{P} - 28.33$	Eqn. 1
		adj.R2 = 0.7102, F = 150.5,df=1,60, p <0.001	
Vulture B		$V_a = 0.004865\mathrm{P} - 29.88864$	Eqn. 2
		adj.R2 = 0.56, F = 34.63, df = 3,75, p<0.001	
Vulture C	Day 1	$V_a = 0.01248P - 95.94$	Eqn. 3a
	Day 2	$V_a = 0.01251304P - 94.464$	Eqn. 3b
	Day 3	$V_a = 0.005662P - 36.13$	Eqn. 3c
		adj.R2 = 0.67, F = 25.6, df = 5,55, p<0.001	
Vulture D	Day 1	$V_a = 0.005014P - 29.766782$	Eqn. 4a
	Day 2	$V_a = 0.003034P - 11.74594$	Eqn. 4b
	Day 3	$V_a = 0.011353P - 88.74803$	Eqn. 4c
		adj.R2 = 0.33, F = 5.55, df = 5,42, p<0.001	

Table S2. Segmented models for climb rate by altitude for each individual. Spearman's rank correlation tests between climb rate and altitude are also given; for low and high thermal regions using data prior to and following the break points identified from their corresponding models.

Bird ID	variable	estimate	Std. error	t	P
A	Intercept	-0.886	0.209	-4.248	<0.001
(Gaelle)	x	0.005	0.001	8.407	<0.001
	u1.x	-0.005	0.001	-7.880	NA
	Adjusted R^2 = 0.383; 4 interactions for convergence				
Estimated break point: 509.85 ± 26.18 m					
Low: r = 0.621, N = 214, p < 0.001; High: r = -0.024, N = 120, p = 0.792					
B	Intercept	-0.827	0.266	-3.109	0.002
(Giselle)	x	0.005	0.001	6.633	<0.001
	u1.x	-0.004	0.001	-5.335	NA
	Adjusted R^2 = 0.361; 3 interactions for convergence				
Estimated break point: 463.13 ± 32.83 m					
Low: r = 0.582, N = 206, p < 0.001; High: r = 0.261, N = 153, p = 0.001					
C	Intercept	-0.402	0.172	-2.340	0.020
(Gregoire)	x	0.004	0.000	7.808	<0.001
	u1.x	-0.003	0.001	-4.300	NA
	Adjusted R^2 = 0.450; 3 interactions for convergence				
Estimated break point: 680.17 ± 69.56 m					
Low: r = 0.451, N = 212, p < 0.001; High: r = -0.069, N = 43, p = 0.657					
D	Intercept	-0.700	0.260	-2.694	0.008
(Hector)	x	0.004	0.001	6.075	<0.001
	u1.x	-0.004	0.001	-2.737	NA
	Adjusted R^2 = 0.330; 2 interactions for convergence				
Estimated break point: 607.00 ± 72.17 m					
Low: r = 0.398, N = 180, p < 0.001; High: r = -0.049, N = 27, p = 0.806					